








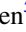







Publication Year	2022
Acceptance in OA	2022-05-09T14:51:59Z
Title	Extending the Baseline for SMC X-1's Spin and Orbital Behavior with NuSTAR Stray Light
Authors	Brumback, McKinley C., Grefenstette, Brian W., Buisson, Douglas J. K., BACHETTI, Matteo, Connors, Riley, García, Javier A., Jaodand, Amruta, Krivonos, Roman, Ludlam, Renee, Madsen, Kristin K., MASTROSERIO, Guglielmo, Tomsick, John A., Wik, Daniel
Publisher's version (DOI)	10.3847/1538-4357/ac4d24
Handle	http://hdl.handle.net/20.500.12386/32096
Journal	THE ASTROPHYSICAL JOURNAL
Volume	926



Extending the Baseline for SMC X-1’s Spin and Orbital Behavior with NuSTAR Stray Light

McKinley C. Brumback¹ , Brian W. Grefenstette¹ , Douglas J. K. Buisson² , Matteo Bachetti³ , Riley Connors¹ ,
Javier A. García¹ , Amruta Jaodand¹ , Roman Krivonos⁴ , Renee Ludlam^{1,8} , Kristin K. Madsen⁵ ,
Guglielmo Mastroserio¹ , John A. Tomsick⁶ , and Daniel Wik⁷ 

¹ Cahill Center for Astronomy and Astrophysics, California Institute of Technology, 1216 E California Blvd, Pasadena, CA 91125, USA; mckinley@caltech.edu

² Department of Physics and Astronomy, University of Southampton, Highfield, Southampton, SO17 1BJ, UK

³ INAF-Osservatorio Astronomico di Cagliari, via della Scienza 5, I-09047 Selargius (CA), Italy

⁴ Space Research Institute of the Russian Academy of Sciences (IKI), Moscow, 117997, Russia

⁵ CRESST and X-ray Astrophysics Laboratory, NASA Goddard Space Flight Center, Greenbelt, MD 20771 USA

⁶ Space Sciences Laboratory, University of California, 7 Gauss Way, Berkeley, CA 94720-7450, USA

⁷ Department of Physics and Astronomy, University of Utah, 115 1400 E., Salt Lake City, UT 84112 USA

Received 2021 November 12; revised 2022 January 6; accepted 2022 January 17; published 2022 February 24

Abstract

StrayCats, the catalog of NuSTAR stray light observations, contains data from bright X-ray sources that fall within crowded source regions. These observations offer unique additional data with which to monitor sources such as X-ray binaries that show variable timing behavior. In this work, we present a timing analysis of stray light data of the high-mass X-ray binary SMC X-1, the first scientific analysis of a single source from the StrayCats project. We describe the process of screening stray light data for scientific analysis, verify the orbital ephemeris, and create both time- and energy-resolved pulse profiles. We find that the orbital ephemeris of SMC X-1 is unchanged and confirm a long-term spin-up rate of $\dot{\nu} = (2.52 \pm 0.03) \times 10^{-11} \text{ Hz s}^{-1}$. We also note that the shape of SMC X-1’s pulse profile, while remaining double peaked, varies significantly with time and only slightly with energy.

Unified Astronomy Thesaurus concepts: X-ray binary stars (1811); High mass x-ray binary stars (733); Pulsars (1306); Neutron stars (1108)

1. Introduction

The Nuclear Spectroscopic Telescope ARray (NuSTAR; Harrison et al. 2013) is the first satellite in orbit that can focus high-energy X-rays between 3–79 keV. The telescope is constructed so that the optics are separated from the detectors by a 10 m open geometry mast. Because the mast is not enclosed, bright sources within 1° – 4° of the focused target can cause stray light, or “aperture flux,” to fall on the detector (see Madsen et al. 2017 for a complete description). Grefenstette et al. (2021) presented StrayCats,⁹ the catalog of stray light observations, and suggested that these observations could be useful in a variety of ways, including performing spectroscopy above 79 keV, reducing telemetry loads for bright sources, and obtaining extra coverage of sources.

Stray light data offer a unique opportunity to increase the observation time of bright X-ray sources, such as accreting X-ray binaries. These sources often go through accretion state changes or exhibit fluctuations in their timing properties that make them interesting to monitor regularly. Stray light observations can offer serendipitous observations of these sources, thereby increasing the baseline of observations for these variable sources.

The high-mass X-ray binary SMC X-1 is an interesting source with which to perform a scientific analysis of stray light data.

This persistently bright source ($L_X \sim 3 \times 10^{38} \text{ erg s}^{-1}$) consists of a $1.21 M_\odot$ neutron star orbiting an $18 M_\odot$ B0 supergiant star (Liller 1973; Falanga et al. 2015). The system is an eclipsing binary with a period of ~ 3.9 days and a binary inclination of $\sim 70^\circ$ (Schreier et al. 1972; van der Meer et al. 2007). SMC X-1 is a frequent stray light source due to its X-ray luminosity and its proximity to other X-ray targets in the Small Magellanic Cloud.

SMC X-1 exhibits X-ray pulsations from the rotation of the neutron star with a period of ~ 0.7 s (Lucke et al. 1976). Long-term studies of the pulse behavior in this source have indicated that the spin frequency is increasing due to accretion torque at a rate of $\sim 2.6 \times 10^{-11} \text{ Hz s}^{-1}$ (Inam et al. 2010; Hu et al. 2019). SMC X-1 also shows an irregular superorbital period of 45–60 days that has long been thought to be caused by warping of the inner accretion disk that obscures the pulsar as the disk precesses (Wojdowski et al. 1998; Clarkson et al. 2003; Brumback et al. 2020). However, more recently there has been evidence that absorption alone is not responsible for the superorbital period and some changes in intrinsic flux may be occurring as well (Pradhan et al. 2020). The most typical superorbital period is about 55 days in length and has a simple sinusoidal shape that defines the source’s high and low states. The duration of the superorbital cycle is quasi-periodic and excursions that bring the period down to 40 days occur roughly every 6 yr (Wojdowski et al. 1998; Clarkson et al. 2003; Hu et al. 2019). These excursions are potentially caused by an instability in the warping of the accretion disk, which changes its geometry as it moves between stable modes (Ogilvie & Dubus 2001; Dage et al. 2019; Hu et al. 2019). These short- and long-term timing behaviors make SMC X-1 particularly interesting to examine through additional stray light observations.

⁸ NASA Einstein Fellow.

⁹ <https://nustarstraycats.github.io/>



Table 1
Description of SMC X-1 Stray Light Observations

ObsID	Stray Light ID	Date	Start Time (MJD)	Exposure (ks)	Module	Stray Light Area (cm ²)
90102014004	10	2015 Oct 12	57,307.91	23.1	FPMA	7.68
90101017002	9	2015 Oct 21	57,316.91	26.7	FPMA	7.73
90201030002	2	2016 Jul 17	57,586.72	54.8	FPMA/B	0.69
90201041002	3	2016 Nov 12	57,704.76	38.6	FPMA	4.31
50311001002	11	2017 Apr 24	57,867.06	153.2	FPMB	5.53
60301029006	8	2017 Nov 17	58,074.69	74.4	FPMA	0.66
30361002002	4	2017 Nov 30	58,087.04	70.7	FPMA	7.08
30361002004	5	2018 Oct 27	58,418.87	58.3	FPMA	6.97

ObsID	Pulse Frequency (Hz)	$F_{3-30\text{keV}}$ (erg cm ⁻² s ⁻¹)
90102014004	1.428669(2)	$(1.91 \pm 0.05) \times 10^{-9}$
90101017002	1.4286958(9)	$(1.98 \pm 0.04) \times 10^{-9}$
90201030002	Not Analyzed ^a	...
90201041002	Not Analyzed ^b	...
50311001002	1.429871(2)	$(1.21 \pm 0.02) \times 10^{-9}$
60301029006	Not Analyzed ^{a,b}	...
30361002002	1.430399(3)	$(1.49 \pm 0.02) \times 10^{-9}$
30361002004	1.431085(2)	$(1.65 \pm 0.03) \times 10^{-9}$

Notes.

^a Stray light pattern covers <1 cm² on detector.

^b SMC X-1's stray light pattern is contaminated by the stray light patterns of other sources.

In this work, we present the first timing analysis of NuSTAR stray light data through eight observations of SMC X-1. We describe the observations, data reduction, and our screening criteria in Section 2. In Section 3 we first use stray light observations that show binary eclipses to confirm the accuracy of the SMC X-1 orbital ephemeris, and then examine the spin behavior and pulse profile shape within our observations. In Section 4 we discuss our results, including the long-term spin behavior of SMC X-1.

2. Observations

StrayCats contains eight observations of SMC X-1 in stray light ranging from 2015 October to 2018 October. We present a brief summary of these observations in Table 1, including both the NuSTAR ObsID and the Stray Light ID from StrayCats. We cleaned and analyzed the data using HEASoft v6.29c, NuSTARDAS v2.1.1, the NuSTAR CALDB v20210921, and the `nustar-gen-utils`¹⁰ software package. For all observations, we reran the NuSTAR pipeline `nupipeline` and extracted a detector image to determine the quality of the stray light. We screened these observations for scientific suitability using the following criteria: the stray light pattern covered more than 1 cm² of the NuSTAR detector and is uncontaminated by overlapping stray light patterns from other nearby X-ray sources.

Following this screening, we found that three of these observations are unsuitable for scientific analysis. Observation 90201030002 shows an extremely small stray light pattern from SMC X-1 that takes up less than 1 cm² on the NuSTAR detector, resulting in too few counts for a scientific analysis. Observations 90201041002 and 60301029006 both have more sizable stray light patterns, but those patterns are contaminated by overlapping stray light emission from other sources. We

show the NuSTAR detector images for these observations and highlight their complications in Figure 1.

For the five remaining observations, we created circular source regions in DS9 that encompassed the stray light pattern on the NuSTAR detector (see Figure 1). When necessary, we also created circular or elliptical exclusion regions centered over the focused target to isolate emission from SMC X-1. We determined the sizes of these exclusion regions visually to encompass the area where the point-spread function surface brightness of the source reached the background level. We performed the barycentric correction on the source-selected event files using the tool `barycorr` with the DE-200 ephemeris and provided the R.A. and decl. of SMC X-1, not the focused target.

3. Analysis

We extracted light curves, source filtered event files, and source spectra using `nustar-gen-utils`. We show the NuSTAR 3–30 keV light curves, binned by 100 s, in Figure 2 as a function of orbital phase. The light curves for Observations 50311001002 and 30361002004 show parts of SMC X-1's binary eclipse. Additionally, Observation 30361002004 also captured a pre-eclipse dip. Such dips have been observed previously in SMC X-1 (Hu et al. 2013) and in a similar accreting pulsar, Her X-1 (Giacconi et al. 1973). In both sources, such dips are likely caused by obscuration of the neutron star by the impact region where the accretion disk meets the accretion stream (Hu et al. 2013).

Before beginning pulsation searches, we first examined where each of the five observations occurred within SMC X-1's superorbital cycle. SMC X-1's X-ray pulsations are often undetected during the superorbital low state due to increased obscuration of the neutron star by the accretion disk (e.g., Pike et al. 2019; Brumback et al. 2020). By examining long-term MAXI (Matsuoka et al. 2009) light curves around the time of our observations, we determined that all five of our

¹⁰ <https://github.com/NuSTAR/nustar-gen-utils>

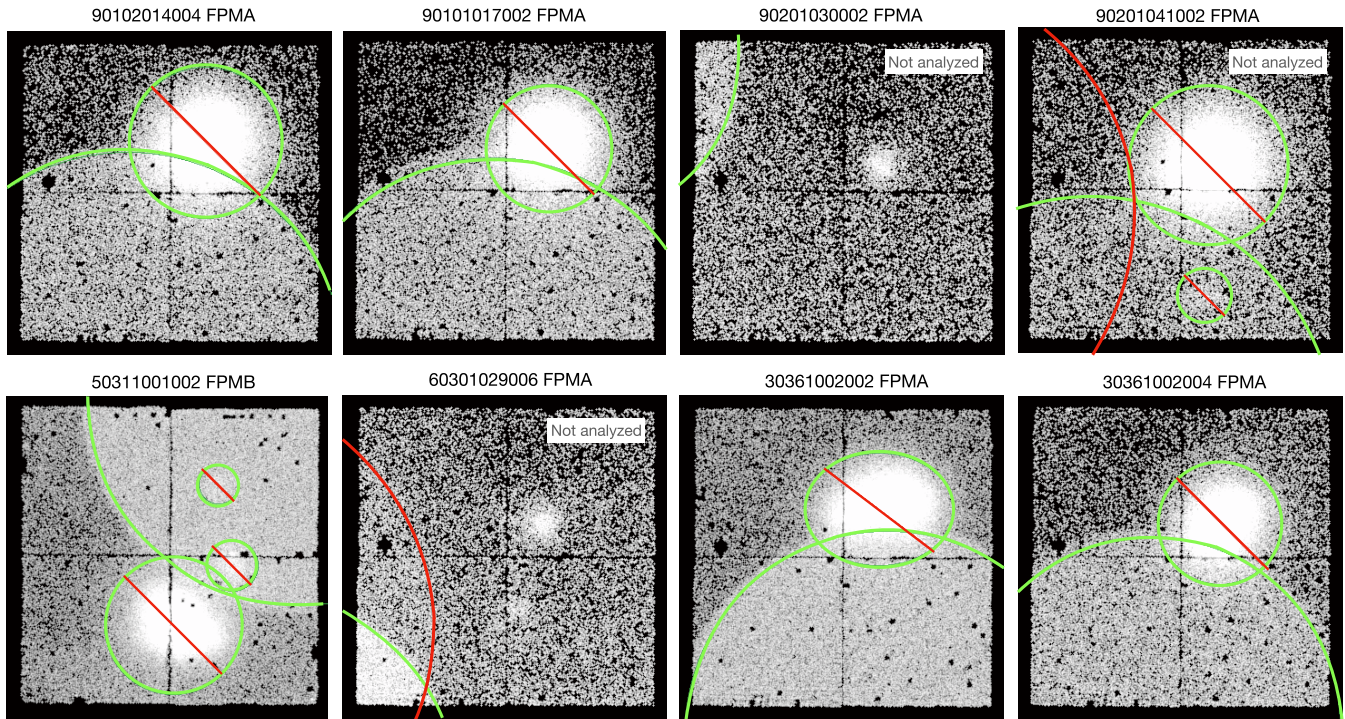


Figure 1. NuSTAR 3–30 keV images in the Detector 1 reference showing the stray light pattern of SMC X-1 in all eight observations within StrayCats. Images have been smoothed with a Gaussian filter. Large green circles indicate the source regions that encompass the SMC X-1 stray light pattern in each observation. In observations where point sources, generally the focused target, overlap the stray light pattern, we remove this emission via exclusion regions (green circle or ellipse with red line). Stray light patterns from sources other than SMC X-1 are shown in red circles. We determined that three of the eight observations were unsuitable for scientific analysis either because the stray light pattern was too small or because of contamination from other stray light sources.

observations occurred within SMC X-1’s superorbital high state, meaning that we could reasonably expect to detect pulsations if the stray light data provided high enough signal-to-noise ratios.

3.1. Verifying the Orbital Ephemeris

As shown in Figure 2, two of our five observations show binary eclipses in their NuSTAR light curves. To our knowledge, the most recent orbital ephemeris for SMC X-1 was determined by Falanga et al. (2015; hereafter F15) with an update to the rate of orbital decay provided by Hu et al. (2019). The rate of orbital decay provided by Hu et al. (2019) differed from the F15 value by 4.7%. Because the two eclipses observed in stray light extended the baseline of observed eclipses from those presented in F15, we tested this ephemeris to see if the orbital parameters had changed. We performed a preliminary test of both the F15 and Hu et al. (2019) ephemerides and found that, for some observations, the F15 ephemeris produced stronger detected pulsations. For this reason, we proceeded with verifying the F15 ephemeris.

We measured the time of the end of the eclipse in Observation 50311001002 and the start time of the eclipse in Observation 30361002004 as the time when 99% of the NuSTAR flux was obscured. We calculated the time of mideclipse using these values and the assumption that the eclipse duration lasts 0.127 of the orbital phase (F15) and found that the times of mideclipse were $57,867.182 \pm 0.032$ MJD and $58,419.775 \pm 0.025$ MJD. It is worth noting that the eclipses used by F15 were observed with INTEGRAL (Lebrun et al. 2003), which has a harder energy range compared to NuSTAR, and thus might have a slightly shorter eclipse duration. We

added these two data points to those presented in Appendix A of F15 for SMC X-1.

Following the work of F15, we used the quadratic orbital change function to predict the time (T_n) of an eclipse an integer number n times after the reference time T_0 :

$$T_n = T_0 + Pn + \frac{1}{2}P\dot{P}n^2$$

where P and \dot{P} are the orbital period and the orbital period first derivative, respectively. In order to isolate and examine the quadratic term and the change in \dot{P} , we plotted the time delay between the observed eclipses and the linear terms of the equation above (Figure 3). We selected T_0 as the mideclipse time of our first observed stray light eclipse (57,867.182 MJD) and fit the time delay data with a quadratic equation, allowing us to solve for the orbital parameters.

We find that the orbital parameters calculated from our fit shown in Figure 3 are consistent with those of F15 forward modeled to the appropriate time. With this consistency, we confirm that the F15 ephemeris for SMC X-1 is still an accurate description of the source’s orbital behavior.

3.2. Selecting Energy Ranges

In order to select the most appropriate energy ranges over which to perform our timing analysis, we examined the 3–100 keV spectra of our five observations. Because stray light does not pass through NuSTAR’s optics, we can examine energies above the calibrated range for focused sources with the accuracy determined by the background and the detector calibration. The reduced signal-to-noise ratio in the stray light observations meant that features such as the Fe $K\alpha$ line, which

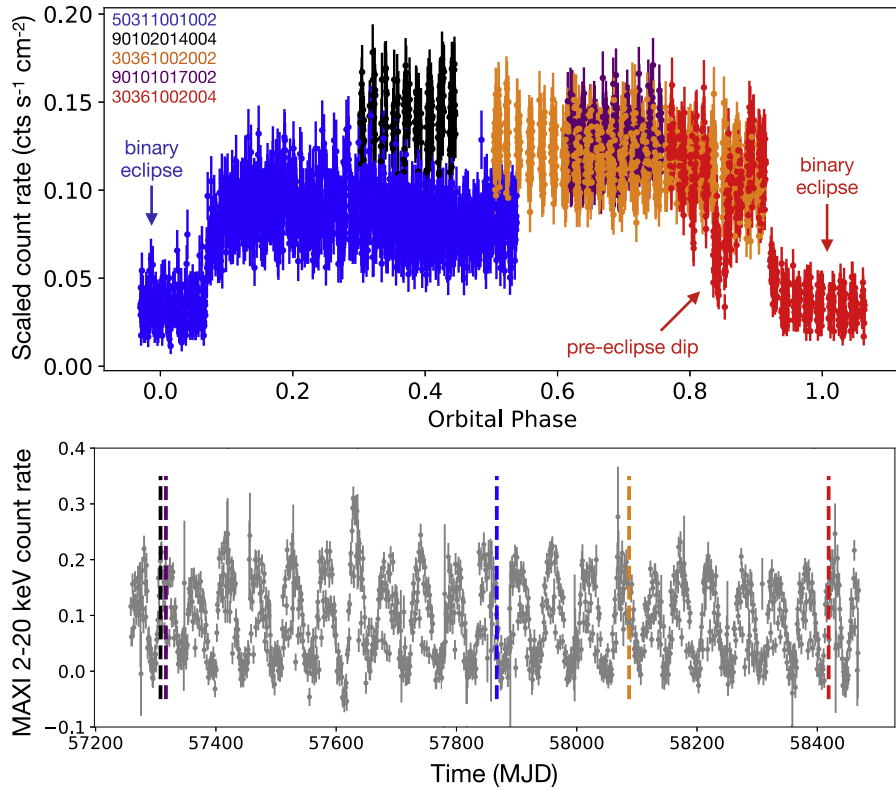


Figure 2. Top: NuSTAR 3–30 keV light curves binned by 100 s for Observations 90102014004 (black), 90101017002 (purple), 50311001002 (blue), 30361002002 (orange), and 30361002004 (red) plotted as a function of orbital phase. The count rates have been scaled by the areas of the respective stray light source regions to highlight source variability. We filtered the light curves to only plot bins with exposure fractions greater than 0.8. Observations 50311001002 and 30361002004 show parts of SMC X-1’s binary eclipse. Additionally, Observation 30361002004 shows a pre-eclipse dip. Bottom: the MAXI 2–20 keV long-term light curve (gray) of SMC X-1 during the three-year interval covered by our observations. The times of stray light observations are indicated with colored dashed lines, where the colors correspond to those used in the top panel.

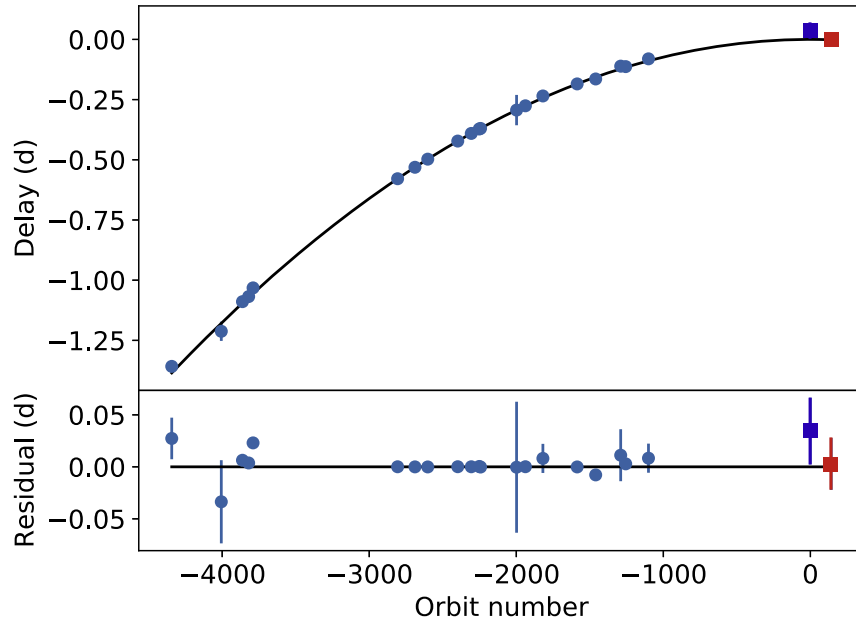


Figure 3. Top: the time delay between the SMC X-1 observed times of mideclipse and the times predicted by the linear terms of the quadratic orbital change equation. Light blue circles are data points from Falanga et al. (2015) and the squares are the two eclipses observed in stray light (Observation 50311001002 in blue and Observation 30361002004 in red). The colors of the squares match the colors of the observation light curves in Figure 2. The black line is the best-fit quadratic equation, which is consistent with the Falanga et al. (2015) ephemeris. Bottom: residuals to the above fit.

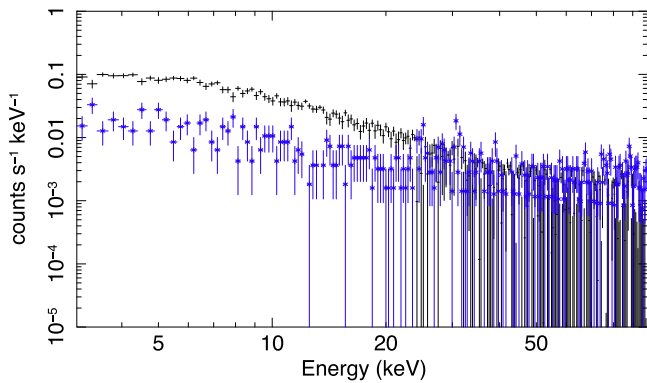


Figure 4. The NuSTAR 3–100 keV stray light spectrum (black) for Observation 90101017002, as a representative example. The source spectrum becomes dominated by the background (blue) at around 30 keV, thus setting an upper energy limit on our timing analysis. The 3–30 keV flux for this and the other analyzed observations can be found in Table 1.

is commonly observed in this source with NuSTAR (e.g., Brumback et al. 2020), were not detected.

For each observation, a circular background region was selected on whichever NuSTAR detector allowed us to find an area away from the focused target and stray light signals. In all observations, we found that the stray light spectrum of SMC X-1 became background dominated at around 30 keV. This value represents a weaker overall source spectrum with respect to the background compared to focused NuSTAR spectra of this source, where the background begins to dominate at ~ 50 keV (e.g., Brumback et al. 2020). As with the lack of an obvious Fe $K\alpha$ line, this is likely due to the reduced signal in stray light.

To illustrate the effect of the background in stray light, we show a representative spectrum from Observation 90101017002 in Figure 4. Examining the point where the spectrum became background dominated allowed us to determine that we would not search for pulsations above 30 keV.

For each of our five observations, we applied a coarse spectral model of an absorbed power law (`tbnew*cutoffpl`) with which to calculate the 3–30 keV flux of each observation. We present these flux values in Table 1. We defer a more detailed spectral analysis to future work.

3.3. Pulsar Spin Frequency Analysis

Following our confirmation of the F15 orbital ephemeris for SMC X-1, we used this solution to correct our observations for its orbital motion.

We used `nustar-gen-utils` to extract event files in the 3–30 keV energy band for each observation for our pulsation search. Using the timing software HENDRICS (Bachetti 2018) and Stingray (Huppenkothen et al. 2019), we created power density spectra (see Figure 5) that indicated pulsations were detected around 1.4 Hz (or the 2.8 Hz harmonic, which is frequently seen in SMC X-1 because of its double-peaked pulse profile) in each observation. We used the HENDRICS epoch folding search to find the best-fit spin frequency and spin frequency first derivative. In all observations, the distribution of the spin frequency first derivative was consistent with zero. We list our best-fit spin frequencies in Table 1. We determined the uncertainty on the spin frequency by using Xselect to extract short time intervals from the start and end of each observation. We created pulse profiles from these start and end

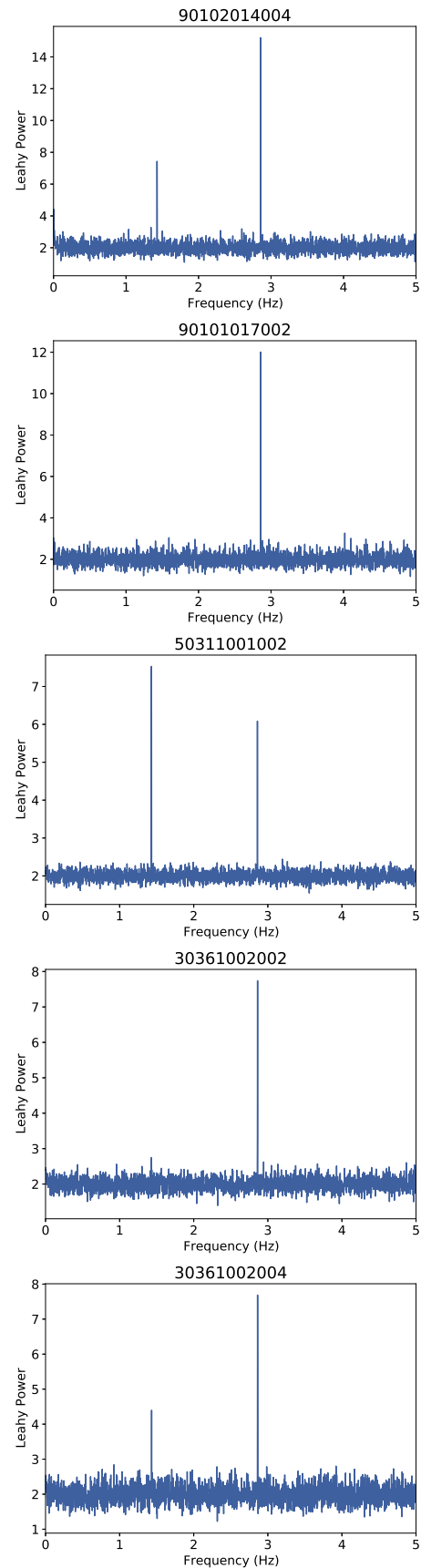


Figure 5. Power density spectra for NuSTAR in the 3–30 keV energy range. In each observation, pulsations at the ~ 1.4 Hz spin frequency and/or its ~ 2.8 Hz harmonic are seen. The harmonic frequency features strongly in SMC X-1’s power density spectra because the pulse profile is double peaked.

time intervals and measured the change in pulse phase between the two. We then calculated our uncertainty in spin frequency as $\delta\nu = \delta\text{phase}/\delta\text{time}$.

The entire observation was used to make the pulse profile except in the case of Observation 50311001002 and Observation 30361002004, in which the data during eclipse were excluded from the pulse profiles. We used Xselect to filter the event files into two energy ranges, 3–10 keV and 10–30 keV, in order to examine energy-dependent changes. We used the `fold_events` tool from Stingray (Huppenkothen et al. 2019) to create the pulse profiles, which are shown in Figure 6.

In the case of Observation 50311001002, our timing analysis indicated small changes in the pulse profile shape as SMC X-1 emerged from binary eclipse. We used Xselect to filter this observation into several shorter time intervals in order to examine the time dependence of the pulse profiles in this observation (Figure 7). We discuss these results in Section 4.

The values in Table 1 indicate that SMC X-1 is spinning up over the course of these observations. We performed a linear regression on the spin frequencies presented in Table 1 and found they indicate a spin-up rate of $\dot{\nu} = (2.52 \pm 0.03) \times 10^{-11} \text{ Hz s}^{-1}$. This value was determined using a least-squares linear regression, which produced a p -value of 2.1×10^{-6} . We show this fit and the resulting residuals in Figure 8 and discuss the implication in Section 4.

4. Results and Discussion

The pulse profiles extracted from our stray light observations of SMC X-1 (see Figure 6) all show the double-peaked profile that is characteristic of this source. We do see some variations between observations, mainly in the relative strength of the weaker secondary pulse. Many previous works examining SMC X-1’s pulse profiles have noted similar changes in the pulse shape with time (e.g., Neilsen et al. 2004; Hickox & Vrtilik 2005; Raichur & Paul 2010). In Figure 6 we show pulse profiles from the 3–10 keV and 10–30 keV energy bands for each observation, although we only see slight differences between the two energy bands. This is consistent with previous studies of energy-resolved pulse profiles in SMC X-1; the double-peaked structure is typically present across the X-ray band, but single-peaked pulse profiles have been seen in the soft X-rays (below 1 keV) where reprocessed emission from the accretion disk dominates (Hickox & Vrtilik 2005; Brumback et al. 2020).

Observation 50311001002 stands out from the others by showing a pulse profile with a significantly weaker secondary pulse (Figure 6). A further investigation revealed variations in pulse profile shape as the pulsar emerges from behind its companion star. We first see this behavior as irregularities in the dynamical z -search of the observation between 3 and 6×10^5 s in the observation, as the source brightens. By extracting pulse profiles in short time intervals over the course of the observation, we see changes in the pulse profile shape from single peaked to double peaked, as well as an overall phase shift (Figure 7, Panel (C)). These changes could be driven by the changing view of the pulsar as it emerges from eclipse, although further modeling of this scenario is needed to confirm this scenario.

Spin-up has been well documented in SMC X-1 since the source’s discovery and is thought to be driven by accretion torques (e.g., Hu et al. 2019). The long-term spin behavior is

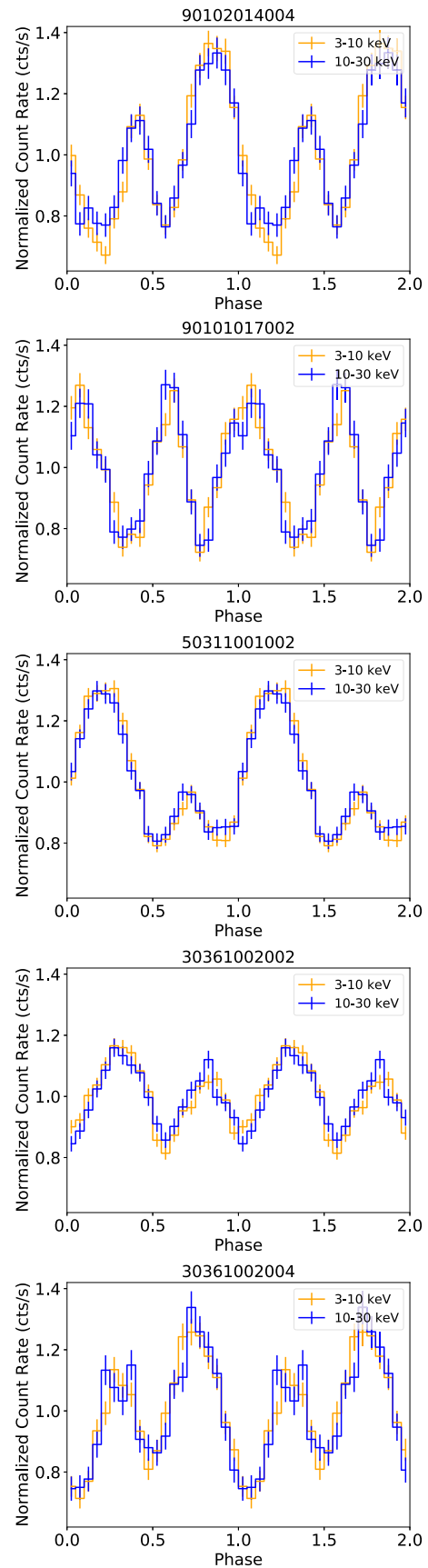


Figure 6. NuSTAR 3–10 keV (orange) and 10–30 keV (blue) pulse profiles for the five observations. These profiles are not phase linked. The y-axis scale is the same in each plot to demonstrate changes in pulsation strength.

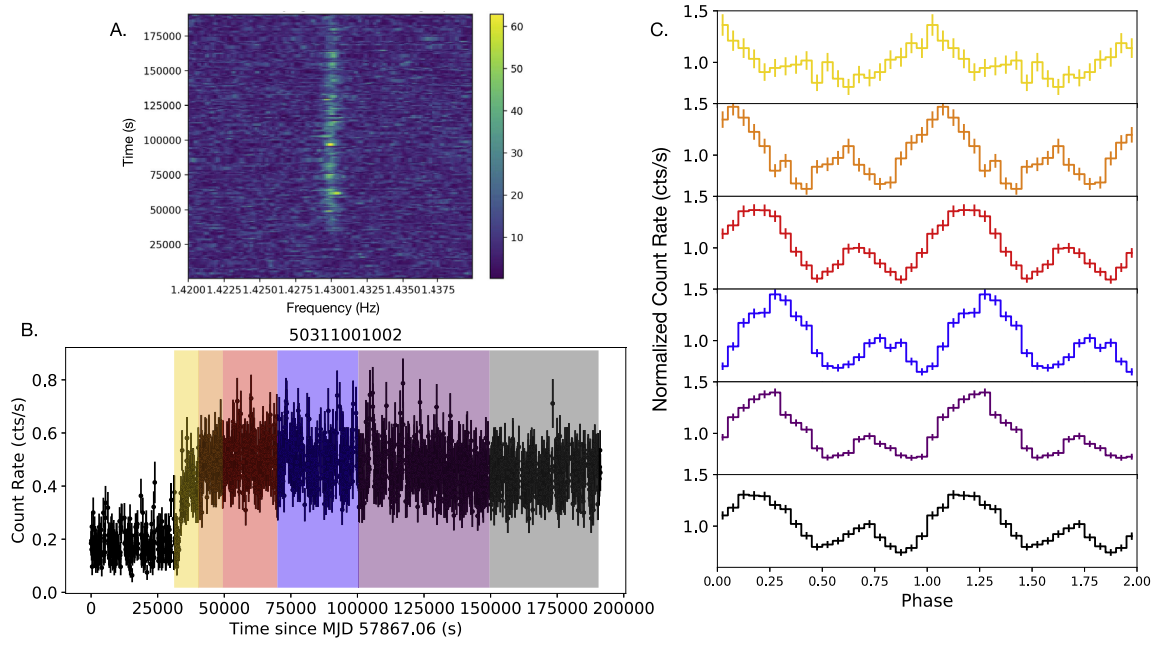


Figure 7. Panel (A): a dynamical z-search of Observation 50311001002 with HENDRICS, where the color indicates the strength of the pulsations with Z_n^2 statistics (Buccheri et al. 1983; Bachetti et al. 2021). The egress from eclipse shows some variations in the strongest pulse frequency, indicating a change in the pulse shape. Panel (B): the light curve of Observation 50311001002 where the colored panels indicate the time intervals from which the pulse profiles in Panel C were extracted. Panel (C): pulse profiles in the NuSTAR 3–30 keV band for each time interval.

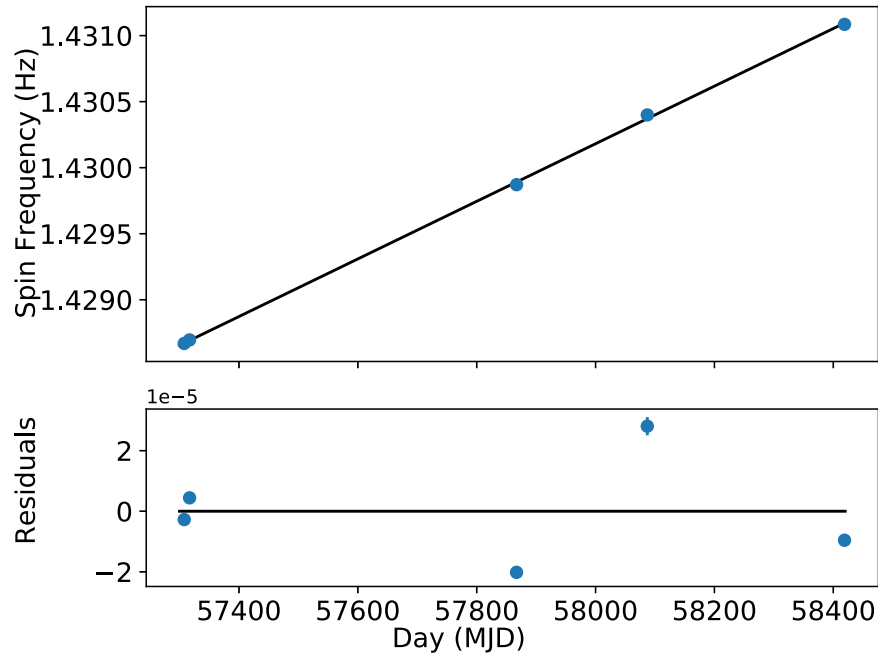


Figure 8. Top: the best-fit linear regression (black) to our spin frequency data from Table 1 (blue points). The fit indicates a spin-up of $\dot{\nu} = (2.52 \pm 0.03) \times 10^{-11} \text{ Hz s}^{-1}$ with a p -value of 2.1×10^{-6} . The error bars are with the point markers. Bottom: residuals to the above fit.

generally linear, although the rate of spin-up appears to vary slightly with time (Inam et al. 2010; Hu et al. 2019; Pradhan et al. 2020). The cause of these variations is not well understood because there are no clear indicators of a change in mass accretion rate (e.g., Inam et al. 2010; Hu et al. 2019). Dage et al. (2019) saw a tentative correlation between spin-up rate and the superorbital period length, possibly due to changing accretion flow that

affected both the disk’s structure and the pulsar’s accretion rate. This conclusion was largely driven by an observed change in SMC X-1’s spin-up behavior around MJD 50,000, which was followed by an epoch of superorbital excursion (Dage et al. 2019; Pradhan et al. 2020).

Our observed spin-up value of $\dot{\nu} = (2.52 \pm 0.03) \times 10^{-11} \text{ Hz s}^{-1}$ is consistent with the spin-up estimations from

Hu et al. (2019) and Pradhan et al. (2020). This agreement indicates that timing analysis of other stray light sources could be used to extend the baseline of pulsation monitoring in similar sources.

5. Conclusions

In this work, we have examined all stray light observations for the high-mass X-ray binary SMC X-1 in the NuSTAR stray light catalog StrayCats. We determined that three of the eight available observations were unsuitable for scientific analysis due to either a small stray light pattern on the NuSTAR detector or contamination from other stray light sources.

For our remaining five observations, we used the `nustar-gen-utils` software to extract data products and performed a timing analysis with these data. Because two observations showed binary eclipses in their light curves, we added these eclipse times to those presented in F15 and confirmed that the orbital ephemeris for SMC X-1 remains unchanged. We performed a pulsation search and found the best-fit spin frequency for each observation, noting a spin-up of $\dot{\nu} = (2.52 \pm 0.03) \times 10^{-11} \text{ Hz s}^{-1}$ across our observations, which is consistent with calculations of the spin-up in this source from focused observations (Hu et al. 2019; Pradhan et al. 2020).











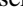


We created pulse profiles in the 3–10 and 10–30 keV energy bands for our five observations (see Figure 6), and explored the time dependence of the pulse profiles in the observation that showed the most unique pulse shape (see Figure 7). We noted that there are significant variations in pulse shape with time, likely caused by the neutron star emerging from binary eclipse.

This is the first scientific analysis of a single source from the StrayCats project. We have demonstrated that NuSTAR stray light observations can be used to obtain good timing solutions and pulse profiles. In particular, stray light observations offer the opportunity to extend baseline monitoring in sources with variable timing properties.

The authors thank the anonymous referee for their time in reading the manuscript and providing helpful comments. M.C. B. would like to thank J. Thorstensen for communication about calculating orbital ephemerides and acknowledges support from NASA funding award No. 80NSSC21K0263. R.K. acknowledges support from the Russian Science Foundation grant 19-12-00369. R.L. acknowledges the support of NASA through the Hubble Fellowship Program grant HST-HF2-51440.001.

Software: HEASoft (v6.29c; HEASARC 2014), NuSTAR-DAS, Stingray (Huppenkothen et al. 2019), HENDRICS (Bachetti 2018), MaLTPyNT (Bachetti 2015), `nustar-gen-utils`.

ORCID iDs

McKinley C. Brumback  <https://orcid.org/0000-0002-4024-6967>
 Brian W. Grefenstette  <https://orcid.org/0000-0002-1984-2932>
 Douglas J. K. Buisson  <https://orcid.org/0000-0002-5341-6929>
 Matteo Bachetti  <https://orcid.org/0000-0002-4576-9337>
 Riley Connors  <https://orcid.org/0000-0002-8908-759X>
 Javier A. García  <https://orcid.org/0000-0003-3828-2448>
 Amruta Jaodand  <https://orcid.org/0000-0002-3850-6651>
 Roman Krivonos  <https://orcid.org/0000-0003-2737-5673>
 Renee Ludlam  <https://orcid.org/0000-0002-8961-939X>
 Kristin K. Madsen  <https://orcid.org/0000-0003-1252-4891>
 Guglielmo Mastroserio  <https://orcid.org/0000-0003-4216-7936>
 John A. Tomsick  <https://orcid.org/0000-0001-5506-9855>
 Daniel Wik  <https://orcid.org/0000-0001-9110-2245>

References

- Bachetti, M. 2015, MaLTPyNT: Quick Look Timing Analysis for NuSTAR Data, Astrophysics Source Code Library, ascl: 1502.021
- Bachetti, M. 2018, HENDRICS: High ENergy Data Reduction Interface from the Command Shell, Astrophysics Source Code Library, ascl:1805.019
- Bachetti, M., Pilia, M., Huppenkothen, D., et al. 2021, *ApJ*, 909, 33
- Brumback, M. C., Hickox, R. C., Fürst, F. S., et al. 2020, *ApJ*, 888, 125
- Buccheri, R., Bennett, K., Bignami, G. F., et al. 1983, *A&A*, 128, 245
- Clarkson, W. I., Charles, P. A., Coe, M. J., et al. 2003, *MNRAS*, 339, 447
- Dage, K. C., Clarkson, W. I., Charles, P. A., Laycock, S. G. T., & Shih, I. C. 2019, *MNRAS*, 482, 337
- Falanga, M., Bozzo, E., Lutovinov, A., et al. 2015, *A&A*, 577, A130
- Giacconi, R., Gursky, H., Kellogg, E., et al. 1973, *ApJ*, 184, 227
- Grefenstette, B. W., Ludlam, R. M., Thompson, E. T., et al. 2021, *ApJ*, 909, 30
- Harrison, F. A., Craig, W. W., Christensen, F. E., et al. 2013, *ApJ*, 770, 103
- Hickox, R. C., & Vrtilek, S. D. 2005, *ApJ*, 633, 1064
- Hu, C.-P., Chou, Y., Yang, T.-C., & Su, Y.-H. 2013, *ApJ*, 773, 58
- Hu, C.-P., Mihara, T., Sugizaki, M., Ueda, Y., & Enoto, T. 2019, *ApJ*, 885, 123
- Huppenkothen, D., Bachetti, M., Stevens, A. L., et al. 2019, *ApJ*, 881, 39
- Inam, S. Ç., Baykal, A., & Beklen, E. 2010, *MNRAS*, 403, 378
- Lebrun, F., Leray, J. P., Lavocat, P., et al. 2003, *A&A*, 411, L141
- Liller, W. 1973, *ApJL*, 184, L37
- Lucke, R., Yentis, D., Friedman, H., Fritz, G., & Shulman, S. 1976, *BAAS*, 8, 441
- Madsen, K. K., Christensen, F. E., Craig, W. W., et al. 2017, *JATIS*, 3, 044003
- Matsuoka, M., Kawasaki, K., Ueno, S., et al. 2009, *PASJ*, 61, 999
- Neilsen, J., Hickox, R. C., & Vrtilek, S. D. 2004, *ApJL*, 616, L135
- Ogilvie, G. I., & Dubus, G. 2001, *MNRAS*, 320, 485
- Pike, S. N., Harrison, F. A., Bachetti, M., et al. 2019, *ApJ*, 875, 144
- Pradhan, P., Maitra, C., & Paul, B. 2020, *ApJ*, 895, 10
- Raichur, H., & Paul, B. 2010, *MNRAS*, 401, 1532
- Schreier, E., Giacconi, R., Gursky, H., Kellogg, E., & Tananbaum, H. 1972, *ApJL*, 178, L71
- van der Meer, A., Kaper, L., van Kerkwijk, M. H., Heemskerk, M. H. M., & van den Heuvel, E. P. J. 2007, *A&A*, 473, 523
- Wojdowski, P., Clark, G. W., Levine, A. M., Woo, J. W., & Zhang, S. N. 1998, *ApJ*, 502, 253